The crustal structure of the NW Moroccan continental margin from wide-angle and reflection seismic data

I. Contrucci,[1] F. Klingelhöfer,[1] J. Perrot,[2] R. Bartolome,[3] M.-A. Gutscher,[2] M. Sahabi,[4] J. Malod[2] and J.-P. Rehault[2]

[1]*IFREMER, Centre de Brest, BP 70, F-29280 Plouzané, France. E-mail: Frauke.Klingelhoefer@ifremer.fr*
[2]*IUEM, Université de Brest, Place Nicolas Copernic, F-29280 Plouzane, France*
[3]*IFP 4, avenue de Bois Preau, F-92852 Rueil-Malmaison Cedex, France*
[4]*Laboratoire Geosciences marines, Faculte des Sciences El Jadida, PO Box 20, 24000 El Jadida, Morocco*

SUMMARY

The Atlantic margin off Morocco with its neighbouring Jurassic oceanic crust is one of the oldest on earth. It is conjugate to the Nova Scotia margin of North America. The SISMAR marine seismic survey acquired deep reflection seismic data as well as wide-angle seismic profiles in order to image the deep structure of the margin, characterize the nature of the crust in the transitional domain and define the geometry of the synrift basins. We present results from the combined interpretation of the reflection seismic, wide-angle seismic and gravity data along a 440-km-long profile perpendicular to the margin at 33–34°N, extending from nearly normal oceanic crust in the vicinity of Coral Patch seamount to the coast at El Jadida and approximately 130 km inland. The shallow structure is well imaged by the reflection seismic data and shows a thick sedimentary cover that is locally perturbed by salt tectonics and reverse faulting. The sedimentary basin thickens from 1.5 km on the normal oceanic crust to a maximum thickness of 6 km at the base of the continental slope. Multichannel seismic (MCS) data image basement structures including a few tilted fault blocks and a transition zone to a thin crust. A strong discontinuous reflection at 12 s two-way travel-time (TWT) is interpreted as the Moho discontinuity. As a result of the good data quality, the deep crustal structure (depth and velocity field) is well constrained through the wide-angle seismic modelling. The crust thins from 35 km underneath the continent to approximately 7 km at the western end of the profile. The transitional region has a width of 150 km. Crustal velocities are lowest at the continental slope, probably as a result of faulting and fracturing of the upper crust. Upper-mantle velocities could be well defined from the ocean bottom seismometer (OBS) and land station data throughout the model.

Key words: gravity, Moroccan margin, wide-angle seismic.

1 INTRODUCTION

The study of passive continental margins is of interest both for understanding the processes of rifting and margin formation, as well as the evolution of associated sedimentary basins. Wide-angle studies of continental margins are used to determine crustal thickness as well as to identify crustal domains (oceanic, transitional, continental) based on velocity–lithology relationships (e.g. White *et al.* 1987; Dean *et al.* 2000). Combined reflection seismic and wide-angle studies offer the stratigraphic information in the basins and the structural images of the upper crust necessary to reconstruct the synrift deformation and subsidence history (e.g. Holbrook *et al.* 1994; Chian *et al.* 1995). When used together, these data can be used to quantify extension in the upper and lower crust, determine the degree of symmetry of rift structures and thus address fundamen-

tal questions concerning the mechanisms of rifting (e.g. McKenzie 1978; Wernicke 1985).

The Atlantic margin off NW Morocco formed during the Triassic—lower Jurassic rifting of the central Atlantic around 180–200 Ma and is one of the oldest margins on earth (Hinz *et al.* 1982; Klitgord & Schouten 1986). While the shallow platform regions have been extensively explored by industry (Heyman 1989; Broughton & Trepanier 1993), the deep portion of the margin is less well studied than that of its conjugate margin in North America off Nova Scotia (Welsink *et al.* 1989; Keen & Potter 1995a). Existing seismic studies have focussed primarily on the southern Moroccan margin (Hinz *et al.* 1982; Weigel *et al.* 1982; Holik *et al.* 1991).

The southern Moroccan margin faces the Canary Islands, a chain of oceanic islands with dated periods of volcanic activity from 35 Ma to present (Hoernle & Schmincke 1993). Seismic studies have

GJI Marine geoscience

determined Gran Canaria and its substratum to be oceanic in nature (Funck *et al.* 1996; Ye *et al.* 1999). Northeast of the Canary Islands, a layer with chaotic seismic facies identified in reflection profiles has been interpreted as volcanic flows derived from the Canary hotspot approximately 40–60 Ma (Holik *et al.* 1991).

As neither a seaward dipping reflectors (SDRs) sequence representing subaerial lava flows nor a high-velocity body at the base of the crust representing underplated material are found at the northern part of the Moroccan Atlantic margin, it is generally considered to be non-volcanic (Mutter 1993). Rifting of the southern margin, however, may have been associated with an older episode of magmatism (Bertrand *et al.* 1982). The oceanic crust adjacent to the Moroccan margin formed in the Jurassic during a period without well marked magnetic reversals and thus no seafloor spreading anomalies older than the M25 magnetic anomaly could be clearly identified in the region (Verhoef *et al.* 1991; Roeser *et al.* 2002).

Earlier workers have identified the S1 magnetic anomaly, which coincides closely to the edge of the salt basin, and interpreted this as marking the ocean–continent boundary (OCB) (Hinz *et al.* 1982; Roeser 1982; Roeser *et al.* 2002). Weak magnetic lineations in the Jurassic crust are oblique to S1 (Verhoef *et al.* 1991; Roeser *et al.* 2002). This suggests a propagation of rifting from the south to the north in agreement with subsidence studies from the Moroccan platform (Le Roy *et al.* 1998). The S1 magnetic anomaly is considered by most authors to be analogous the the East Coast Magnetic Anomaly (ECMA) off the east coast of North America (Hinz *et al.* 1982; Klitgord & Schouten 1986) and to mark the OCB. S1 is difficult to follow north of 33.3°N. Likewise, the ECMA diminishes in intensity and disappears just south of 44°N on the Nova Scotia margin (Keen & Potter 1995a,b). The ECMA is typically interpreted as representing large-scale extrusive volcanism or underplating related to the breakup of the continental lithosphere. Along several transects, the ECMA is spatially related to ≥ 10-km-thick sequences of SDRs and is thus considered to be indicative of a volcanic margin (Holbrook & Kelemen 1993; Holbrook *et al.* 1994). This raises an important question: does the northward termination of these magnetic anomalies mark the transition from a volcanic margin to a non-volcanic margin?

With these objectives in mind, in 2001 April, a two-ship seismic survey acquired over 3000 km of MCS data and 1000 km of wide-angle profiles on the central and northern Moroccan margin (Fig. 1). The main goals of the SISMAR project were to image the deep structure of the margin, characterize the nature of the crust in the transitional domain and define the geometry of the synrift basins. One priority was to survey the deep salt basin off northern Morocco and its relation to the continent–ocean transition. A further goal was to study the tectonic reactivation of the margin. The profiles in the northern portion of the study area sample a
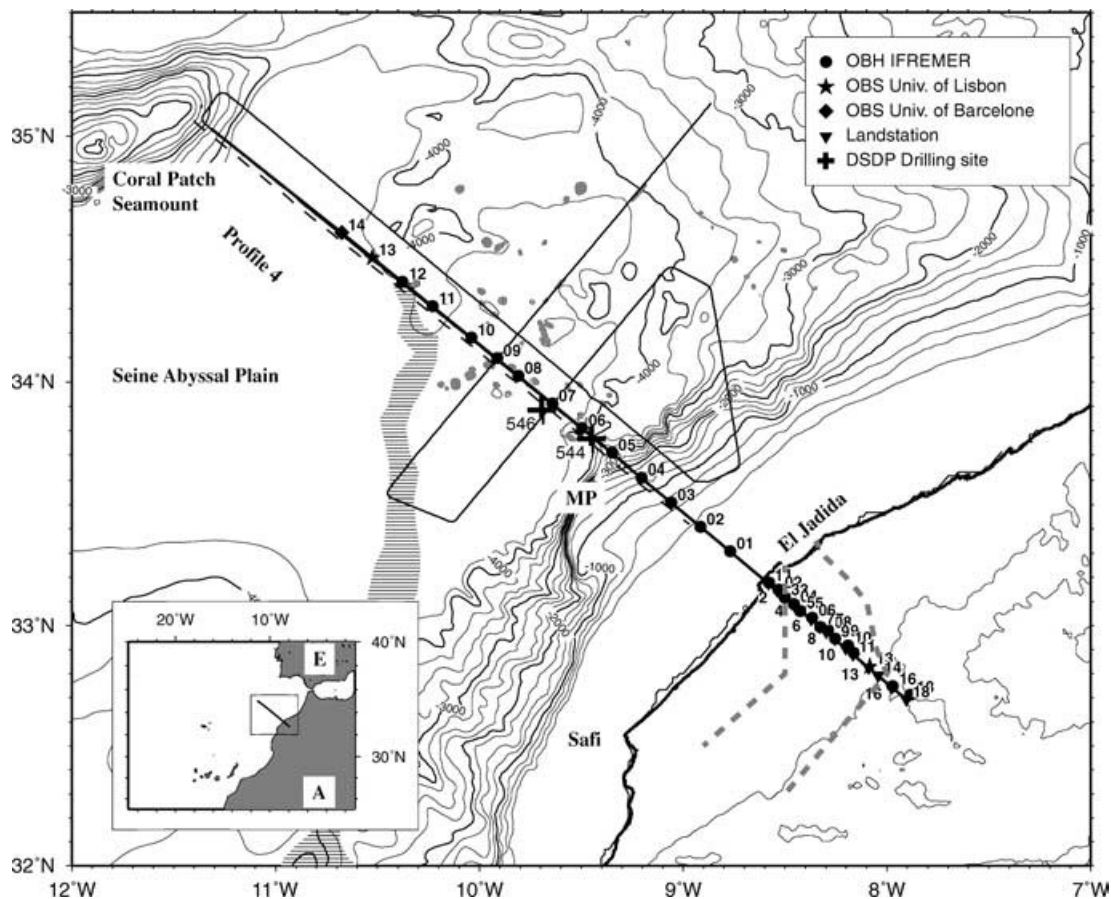

Figure 1. Predicted bathymetry from satellite gravity of the study area at the Atlantic margin off Morocco (Smith & Sandwell 1997). Circles mark Ifremer OBH positions, a star the position of the OBS of the University of Lisbon, a diamond the position of OBS of the University of Lisbon, inverted triangles positions of the land stations and crosses DSDP drilling sites from Leg 79. The bold black line marks the profile presented in this paper, thin lines position of neighbouring profiles and broken line position of the reflection seismic profile. Thick, broken grey line indicates the extent of the El Jadida basin in the vicinity of the land stations, vertically striped area the position of the S1 magnetic anomaly and horizontally striped areas the position of salt diapirs in the basin. MP = Mazagan plateau. Inset shows the regional setting of the study area. A = Africa, E = Europe.

region of active deformation along the Africa–Iberia plate boundary (Sartori *et al.* 1994). Here, basin inversion has occurred as expressed by folding and reverse faulting of the sediments. Furthermore, large-scale deformation of the oceanic crust has produced large bathymetric highs (e.g. Coral Patch, Ampere seamounts, Gorringe bank). The first results of the northern area, including the discovery of an active accretionary wedge complex have been reported elsewhere (Gutscher *et al.* 2002).

The structure of the rifted margin is examined below along a transect orthogonal to the Moroccan margin, crossing the base of the continental slope at the northern edge of the Mazagan plateau (Hinz *et al.* 1982; Ruellan & Auzende 1985). This transect extends from oceanic crust in the Seine abyssal plain (to the NW) to unthinned continental crust 100 km SE of the coast. Deep sea drilling was performed at the base of the Mazagan plateau during Leg 79 (Hinz *et al.* 1984). Site 544 penetrated granitic gneiss beneath a NE trending ridge on the seafloor at 3600 m water depth clearly establishing its nature as a tilted fault block. Site 546, drilled at 3960 m water depth on a morphologic high 20 km further west penetrated a salt diapir (Fig. 1).

2 DATA ACQUISITION AND PROCESSING

In this study, we present results from the combined interpretation of seismic reflection and wide-angle data on a 440-km-long profile extending from nearly normal oceanic crust in the vicinity of Coral Patch seamount to the coast at El Jadida and approximately 130 km inland (Fig. 1). 12 ocean bottom hydrophones (OBH) of Ifremer, one OBS of the University of Lisbon and one OBS of the University of Barcelona were deployed, all of which yielded good data. The marine shots were successfully recorded by 14 land stations (HATHOR Leas) of the network of the Institut National des Sciences de l'Univers (INSU). Most of the land stations (N3 to N14) were located in the El Jadida basin (Le Roy *et al.* 1998). Land stations N1 and N2 close to the coastline were situated on the Oualidia horst and land land-stations N15 and N16 on metamorphic basement (Fig. 1). 1957 shots were fired from a 4850 in^3 (79 litre) airgun array at a shot spacing of 150 m. The source was tuned to single bubble mode to enhance low frequency and allow deep penetration (Avedik *et al.* 1993). Most of the profile was reshot using a smaller (2369 in^3; 38.8 litre) source tuned to the first peak to enhance the resolution of the image for the sedimentary layers. Both the single bubble and the first peak MCS profiles were recorded using a 4.5-km-long, 360-channel streamer, yielding 15-fold trace coverage. OBH, land station and seismic streamer data were recorded at a sample rate of 4 ms. No reflection seismic data could be acquired east of OBS 02 as a result of the shallow water depth.

Processing of the MCS data was performed using the GEOVECTEUR processing package. It included spherical divergence correction, frequency wavenumber filtering, bandpass filtering (3–5–50–60 Hz), internal mute and dynamic corrections. Velocity analysis was performed every 200 common depth point for the final stack. The last processing step included applying an automatic gain control and a Kirchoff migration using water velocity (Fig. 2). The sedimentary layers often disturbed by salt tectonics are well imaged in the reflection seismic section. The basement reflector is clearly distinguishable throughout the section, except directly underneath the salt diapirs. Reflections from the Moho are scarce and confined to the western half of the profile.

Pre-processing of the OBS data included calculation of the clock-drift corrections (between 0–4 ms per day) to adjust the clock in

each instrument to the GPS base time. Instrument locations were corrected for drift from the deployment position during their descent to the seafloor. After this correction, the instrument locations are between 0 and 100 m off the line, which does not affect the interpretation, as the true source–receiver offsets are used for the modelling.

The two OBSs (14 and 13) as well as the three westernmost OBHs (12, 11, 10) display an excellent data quality with clear arrivals up to an offset of 100 km (Fig. 3). Data quality decreases slightly eastwards as a result of a thick layer of salt that prevents penetration of the acoustic energy down to deeper crustal layers. The presence of fault blocks and tectonically disturbed sediments complicates picking and phase identification at the continental slope. All land stations gave very good data with clear arrivals at offsets up to 200 km (Fig. 4).

3 SEISMIC VELOCITY MODELLING

Picking of first and later arrivals was performed without filtering where possible (mostly between offsets of 0–40 km). Different filters were applied to the data where necessary, depending on the quality of the data and offset to the source, as arrivals from longer offsets are of lower frequency compared to short-offset arrivals. Estimated picking uncertainties for the OBS data were 30 ms for the direct water wave, 50 ms for all sedimentary arrivals, 60–80 ms for crustal arrivals and 80–120 ms for arrivals from the Moho and mantle. Picking uncertainties for the land station data were chosen to be larger because of the larger offset between the instrument and the shots, 100 ms for the crustal arrivals and 150 ms for the arrivals from Moho and upper mantle.

The data were modelled using the combined forward and inverse modelling software package RAYINVR (Zelt & Smith 1992). The layer stripping approach was used and layers were modelled from the top of the model downwards. Upper layers, which were not directly constrained by arrivals from within the layer, were adjusted to improve the fit of lower layers. The seafloor bathymetry was taken from the ship sonar data and sampled at an lateral interval of 0.5 km to include it in the model. Arrival times of the main sedimentary layers and basement were picked from the reflection seismic data and included in the model at an lateral interval between 0.5 and 2.5 km, depending on the topography and depth of the layer. The arrival times were converted to depth using the OBS data and velocities consistent with those from velocity analysis of the reflection seismic data were achieved (Bartolome *et al.* 2004). The depth and velocities of the crustal layers and the upper mantle were modelled from the OBS data.

Correspondingly, the wide-angle seismic model converted to a two-way traveltime model show good agreement with the reflection seismic section (Fig. 2). Velocities of the main sedimentary layers were constrained by wide-angle seismic data, but some additional layering is imaged by the reflection seismics. Depth of the basement is in very good agreement along the complete model and differences in the depth to the Moho are generally smaller then the expected accuracy of the wide-angle model of approximately ± 1 km at the depth of the Moho. The wide-angle seismic Moho corresponds to the first of a series of deep reflections found in the reflection seismic section. Node interval in the deeper layers was chosen between 6 and 10 km.

The final velocity model consists of three sedimentary layers modelled with velocities of 1.6–1.7 km s^{-1} for the shallowest layer, typical for young sediments with a high water content, 2.8 to 3.0 km s^{-1} for an intermediate sedimentary layer and 3.7–3.9 km s^{-1}
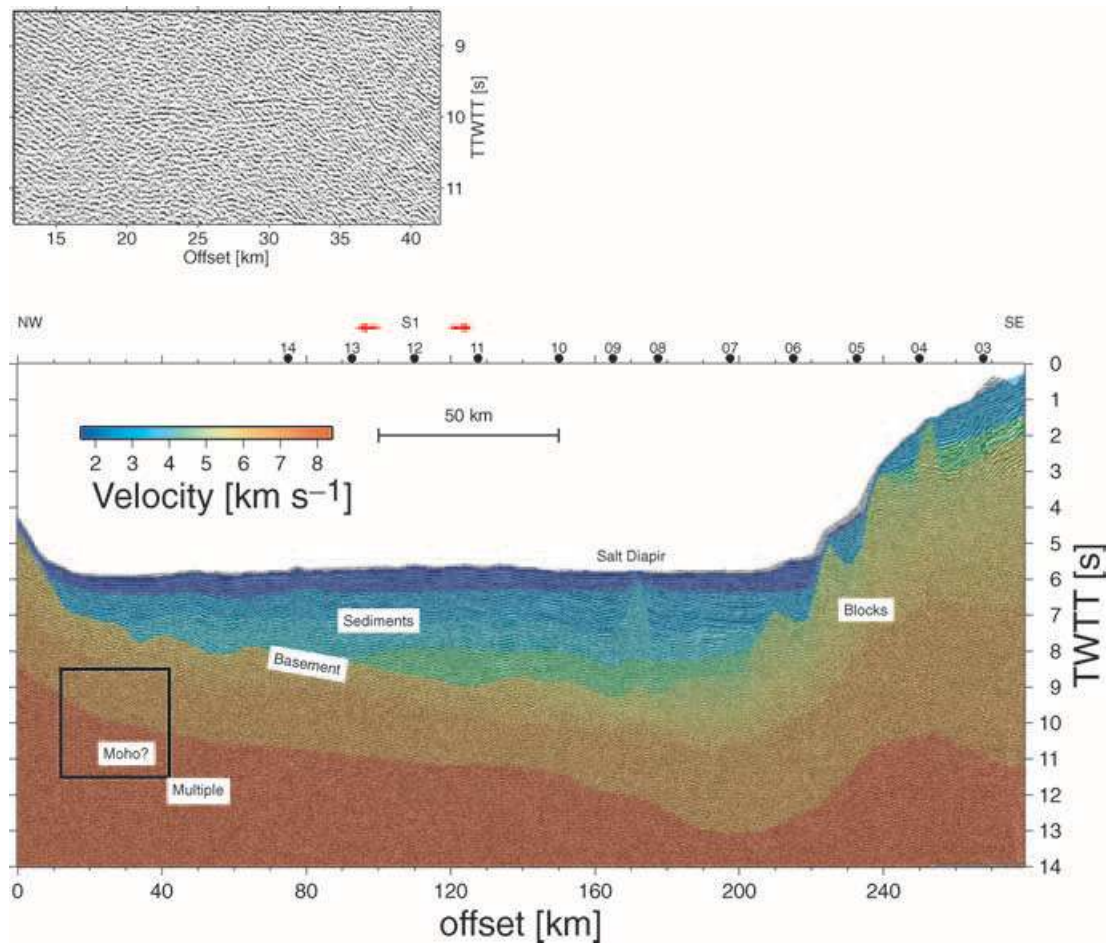
Figure 2. Migrated mulichannel seismic section, with velocities from wide-angle modelling underlain. OBS positions are indicated by circles and S1 anomaly by red arrows. Blow-up is marked by black triangle.

at the deepest parts of the model, probably consisting of older, load compacted, sediments (Fig. 5a). One sedimentary layer showing dome-like structures was modelled using a velocity of 4.4–4.8 km s^{-1}, typical velocities for salt layers. The geometry of the sedimentary layers shows good agreement with the reflection seismic data, although not all details of the layers are fully resolved by the OBS data. The sediments and the basement are gently updomed at approximately 110 km model distance. Two crustal layers in the oceanic or thinned continental crust parts of the model were modelled with velocity gradients from 6.2–6.4 and 6.6 to 6.8 km s^{-1}. At the continental slope area, the velocity of the upper crustal layer is reduced to 5.6 km s^{-1}. The crustal thickness increases eastwards from around 8 km at Coral Patch seamount to 35 km underneath the continent. Beneath this part of the model, a third crustal layer was modelled displaying a velocity of 7.0 to 7.4 km s^{-1}. The upper-mantle layer displays velocities from 8.0 to 8.3 km s^{-1} constrained by numerous P_n arrivals along the profile.

4 ERROR ANALYSES

Velocity gradients and the phase identification in the velocity model were further constrained by synthetic seismogram modelling using asymptotic ray theory (Zelt & Ellis 1988). The synthetic seismograms generally show a good agreement with the recorded sections, especially in the oceanic domain (Fig. 3b) and for the land stations (Fig. 4b).

The χ^2 error is a measure of the quality of the fit between the picked data points and the predicted arrival times from the velocity model (Fig. 6). It is defined as the rms traveltime misfit between calculated and observed arrivals normalized to the picking error. The number of picks, picking error, the values for the χ^2 parameter and the rms misfit for all phases are listed in Table 1.

The sedimentary layers are well constrained by the OBS data (Fig. 6a). The crustal and upper-mantle structure is constrained by reflections and refractions from the OBS and land station data (Figs 6b, c and d). Additional information about the quality of the model can be gained from the resolution parameter (Fig. 7). This parameter is a measure of the number of rays passing through a region of the model constrained by a particular velocity or depth node and is therefore dependent on the node spacing. Values greater than 0.5 are considered to be well resolved. Generally the model is well constrained, with values greater than 0.5 for the most of the crustal and sedimentary layers as well as the upper mantle. The subaerial El Jadida basin between 320 and 380 km model distance shows a low resolution, mainly as a result of the lack of short-offset information for the land stations. The first sedimentary layer is poorly resolved, because no turning rays in this layer could be detected in the data sections, as a result of their very short offsets. The salt diapir at 250 km model offset is not resolved by the wide-angle data and its geometry has been taken from the reflection seismic section. The third sedimentary layer and the lower crustal layer underneath the continent show a slightly lower resolution than the rest of the model,
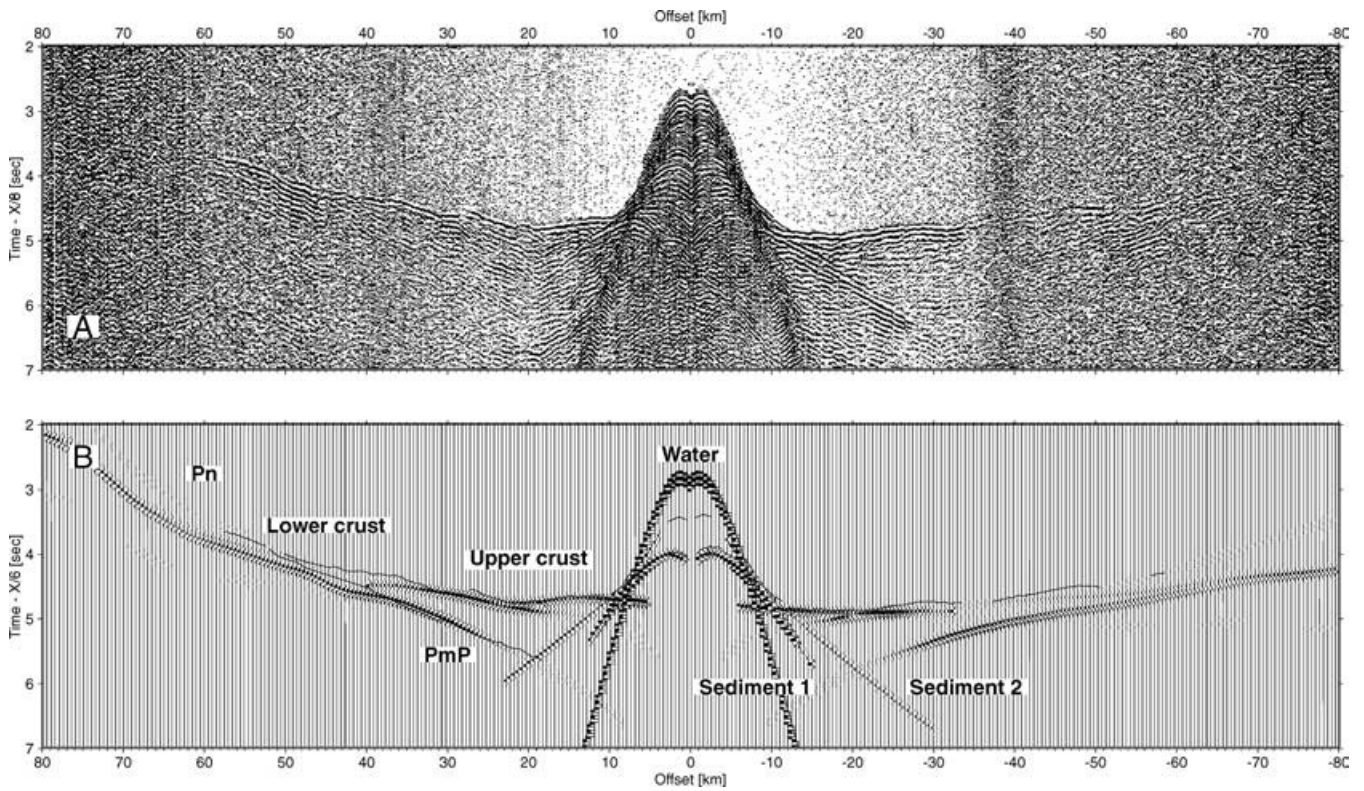
Figure 3. (a) Bandpass filtered (3–5, 24–36 Hz) data from OBS 14. The data are displayed with gain proportional to source–receiver offset and are reduced at a velocity of 6 km s^{-1}. (b) Synthetic seismograms calculated from the model for the same station using asymptotic ray theory (Zelt & Smith 1992). The synthetic seismograms are spaced at a 500-m interval and the same offset-dependent gain has been applied as in (a). The source wavelet consists of a 29-point low-pass filtered Ricker wavelet. *P*-wave quality factors were chosen to be 100 for sedimentary layers, 650 for the crustal layers and 1000 for the upper mantle. Black lines represent traveltime picks.
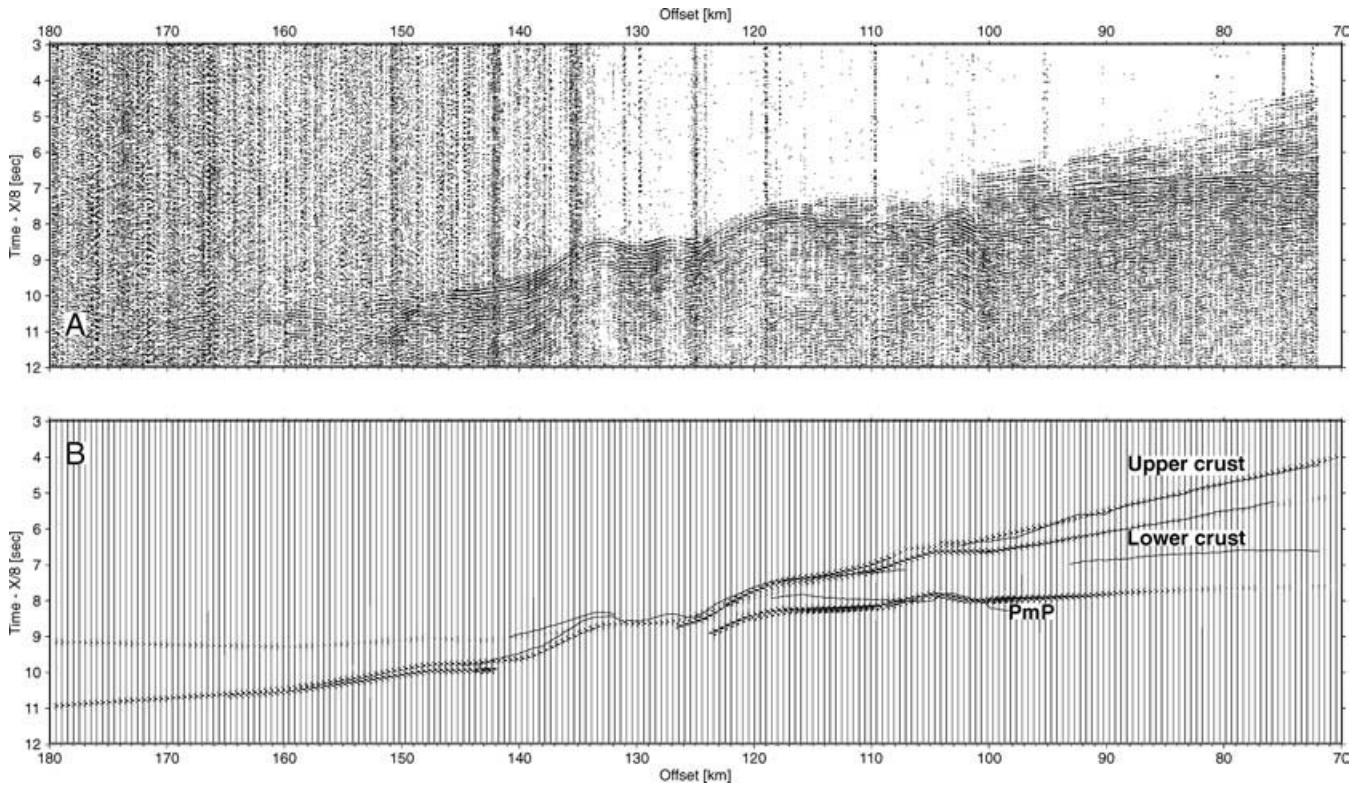

Figure 4. (a) Data from land station 07 for the profile with same gain, filter and scaling applied as in Fig. 3. (b) the corresponding synthetic seismograms.
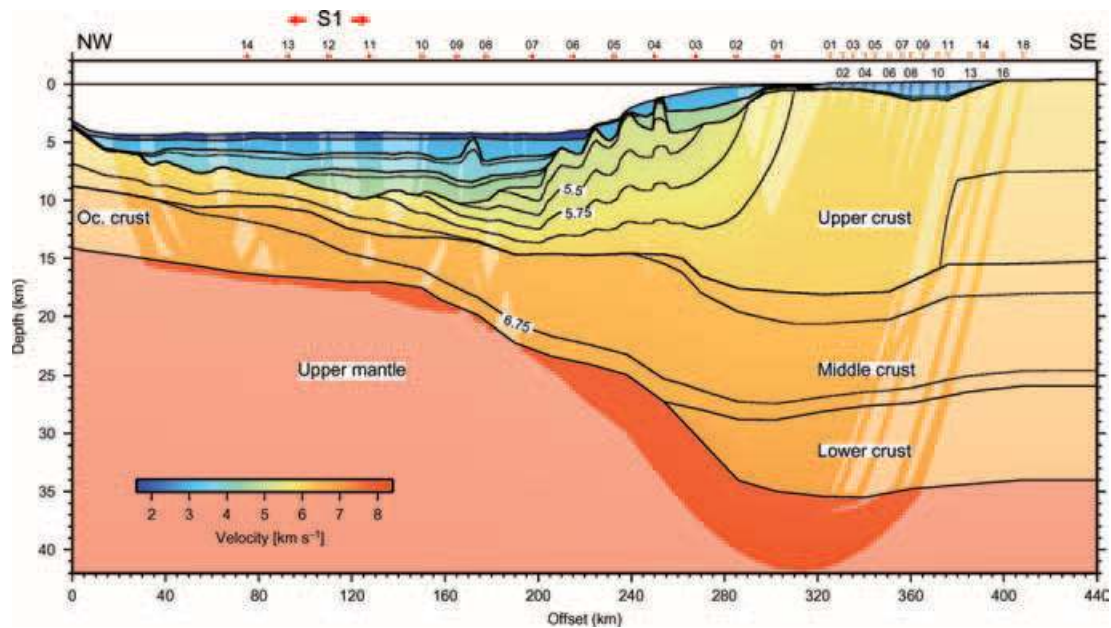
Figure 5. (a) Final velocity model of profile 4 including the model boundaries used during inversion (solid lines) and isovelocity contours every 0.25 km s^{-1}. Positions of OBH/OBSs (circles) and land stations (inverted triangles) indicated. Darker shaded areas show ray paths from the modelling and hence regions of the model that are constrained. Cross-point of the profile with the S1 magnetic anomaly is indicated.

which is explained by the fact that both layers are mainly modelled from reflected arrivals, as no turning rays from these layers could be picked.

The depth uncertainty of the main model layers has been assessed through a perturbation of the depth of the layers. Using the F-test, the 95 per cent confidence interval has been determined at which the perturbed and the original model are significantly different (Fig. 7).

5 GRAVITY MODELLING

Because seismic velocities and densities can be correlated, gravity modelling provides important additional information on the seismic model. Areas unconstrained by the seismic data can be further constrained by gravity modelling.

In a first step, the mean layer velocities from the seismic model were converted to densities using the empirical relationships from Ludwig *et al.* (1970), Hamilton (1978) and Hughes *et al.* (1998) for the sedimentary layers and the relationship of Christensen & Mooney (1995) for crustal layers (Fig. 8). Layers from the velocity modelling have only been subdivided where necessary and strong lateral velocity gradients are present. The upper-mantle densities are set to a constant 3.32 g cm^{-3}, consistent with the upper-mantle velocity of 8.00–8.20 km s^{-1} found from the seismic data. To optimize the fit of the final gravity model (Fig. 8), the densities of each layer were subsequently manually varied within an error bound of 0.25 g cm^{-3} from their original value. This deviation is considered a realistic uncertainty of empirical relationships used for the velocity–density conversion.

The gravity anomaly along the profile has been extracted from the free-air gravity data set obtained by satellite altimetry of Sandwell & Smith (1995) (Fig. 9). The gravity data were forward modelled using the GRAVMAG gravity and magnetic modelling software developed by the British Geological Survey (Pedley *et al.* 1993). The resulting gravity model of the profile consists of 11 polygons each with constant density (Figs 10a and b). To avoid edge effects, the

model has been extended 200 km at both ends and down to a depth of 95 km.

The sedimentary layers have been assigned a density of 2.10, 2.35 and 2.40 g cm^{-3}. The fact that the model does not require a layer of relatively low density indicates that the salt does not form a massive layer and the percentage of salt even in the diapirs is low. The density of the upper crust is 2.65 g cm^{-3} and of the lower crust is 2.90 g cm^{-3}. These values are in good accordance with values for continental crust (Christensen & Mooney 1995). The low-velocity area of the upper crust in the vicinity of the fault block has been assigned a corresponding lower density of 2.50 g cm^{-3}. The resulting predicted gravity anomaly along the profile shows a good fit to the satellite observed gravity. The largest misfit can be observed at the westernmost end of the model and probably results from Coral Patch seamount. The large negative anomaly around 210 km model distance can be predicted in amplitude, however the maximum is shifted slightly to the NW, which might be a result of the three-dimensional basement topography in this area.

To verify if the model is isostatically balanced, the load anomaly has been calculated (Fig. 10c) along the profile. The out-of-plane stresses do not exceed 10 bar, which can be sustained by the crust (Whitmarsh *et al.* 1996).

6 NATURE OF THE CRUST IN THE TRANSITIONAL DOMAIN

One of the main aims of the SISMAR seismic experiment was to define the nature of the crust in the transitional zone and to locate and quantify the occurrence of serpentinized mantle material present in the crust. Serpentinized mantle material at the depth of the lower crust or upper mantle characteristically displays seismic velocities between 7.0 and 7.6 km s^{-1}, which is in between those of lower crustal gabbros (6.5–6.8 km s^{-1}) and those of normal mantle material (8.0–8.2 km s^{-1}). Velocities >7.3 km s^{-1} are for example consistent with <25 per cent serpentinization of mantle peridotite (Miller & Christensen 1997). No such
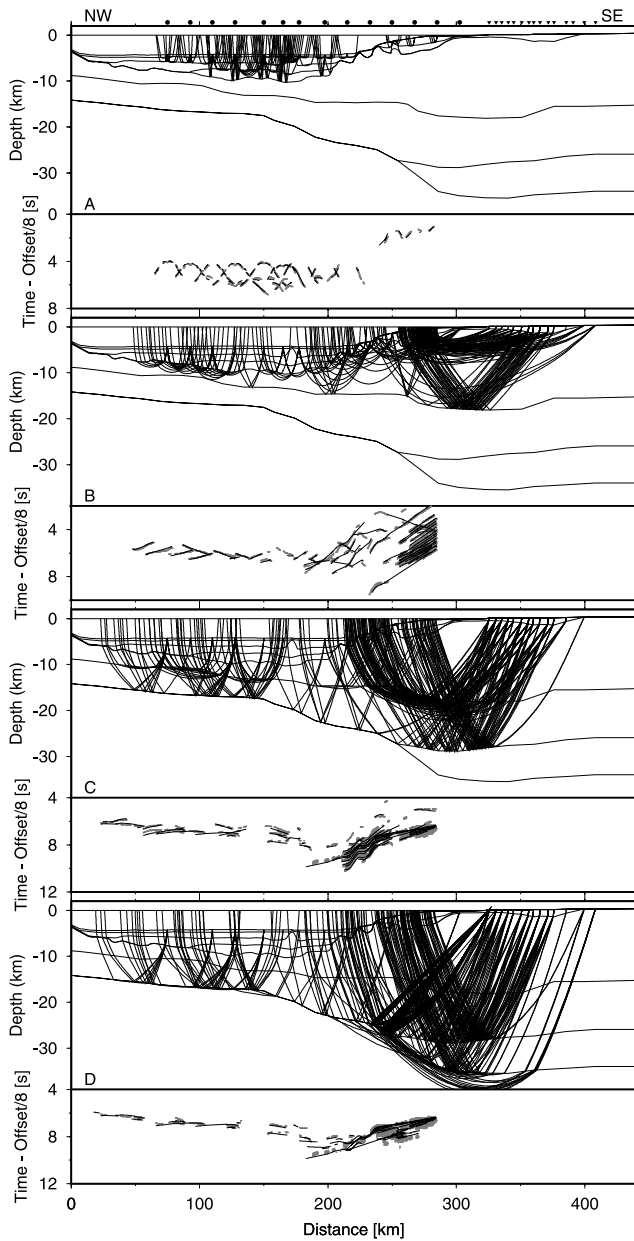
Figure 6. (a) Upper panel: ray coverage of the model for the sedimentary layers, with every 20th ray from point-to-point ray tracing. Positions of the receivers are indicated by inverted triangles and circles. Lower panel: fit between the traveltime picks (dark grey bars) and the predicted arrival times (black lines) from ray tracing for the sedimentary layers. (b) As in (a) for the upper crustal layer. (c) As in (a) for the middle and lower crustal layer. (d) As in (a) for the lower crustal and upper-mantle layer.

Table 1. Traveltime residuals and chi squared error for each phase and the complete model.

	No. of picks	rms	Chi squared
Water	1871	0.035	1.074
Sed. 1	223	0.108	4.701
Sed. 2	384	0.069	1.932
Sed. 2 refl.	251	0.058	1.350
Sed. 3	225	0.073	2.126
Sed. 3 refl.	225	0.073	2.126
Upper crust	3254	0.115	2.769
Mid-crustal refl.	903	0.104	1.375
Lower crust	2058	0.151	2.499
P_mP	2002	0.144	1.464
P_n	852	0.177	1.793
All Phases	13120	0.132	2.193

the data is found between both models. The possibility of significant variances between both models is only 16 per cent.

To further investigate the problem, synthetic seismograms have been calculated using both models (Fig. 11). The lower amplitude of the arrivals from the lower crust and the stronger P_mP reflection seem to support the hypotheses that the lower crust is gabbroic than serpentinised upper-mantle material. Also, the fact that the that the higher gradients in the lower crust lead to a fading out of arrivals from the layer earlier than seen in the data supports the crustal nature inferred from the final velocity model.

7 DISCUSSION

7.1 The ocean–continent boundary

The final velocity model (Fig. 5) shows a 35-km-thick continental crust, which thins to approximately 7 km over a distance of 150 km (near OBS 10). If the crust at OBS 10 is continental in nature, then this implies an extension factor of $\beta = 5$. Indeed, several lines of evidence favour crust of continental affinity there. The velocity gradients in the upper crust suggest that normal oceanic crust begins NW of OBS 12 or 13. Also, a layer of high-velocity sediments probably representing the pre-rift basin infill disappear west of OBS 12 (Fig. 2), probably indicating the ocean-continent boundary. The character of the basement relief changes between OBS 12 and 13 from a smooth to a rougher surface more characteristic of oceanic basement.

Magnetic anomalies of moderate amplitude (20 nT) at OBS 9 and 12 may represent the prolongation of the S1 magnetic anomaly. Along the majority of the Moroccan margin, the seaward edge of the salt diapir province corresponds spatially to the ocean–continent boundary as identified on from seismic velocities and magnetic anomalies (Hinz *et al.* 1982; Roeser *et al.* 2002). A salt diapir penetrates the seafloor between OBS 8 and 9 and a smaller amplitude diapir is imaged by the MCS data just NW of OBS 10. Salt diapirs identified from other reflection seismic profiles are located close to OBS 12 and 13, southeast of the prolongation of the S1 anomaly through OBS 12 indicating a location of the ocean–continent boundary between OBS 11 and 13 (Sahabi *et al.* 2004). Downward migration of the salt layer over the ocean–continent boundary onto oceanic crust as has been found for the conjugate margin of Nova Scotia (Keen & Potter 1995a) would be associated with sedimentary faulting. However, this is not observed in our study area.

This interpretation is in good agreement with the wide-angle seismic model, which shows a two-layered crust with velocities
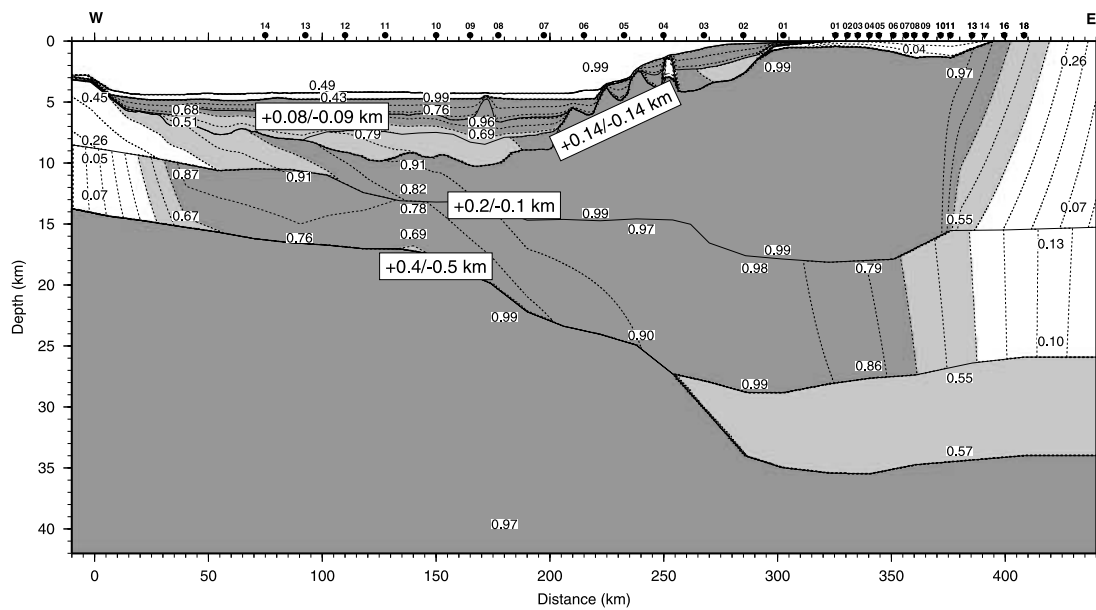
zone has been included in the final velocity model. To answer the question whether this is the result of the data quality, which does not allow the zone of anomalous seismic velocities to be resolved, or whether the lack of anomalous velocities are constrained by the data, an alternative velocity model has been constructed including a layer of higher seismic velocities between the continental and pure oceanic domains (Fig. 11). By deepening the Moho discontinuity, it was possible to find an equally good fit between the predicted and observed traveltimes as for the final velocity model. The F-test demonstrates that no significant difference in the traveltime fit of

Figure 7. Resolution for the velocity nodes. White regions indicate poorly constrained areas (resolution lower than 0.5), light grey shading indicates well constrained areas (resolution between 0.5 and 0.7) and dark grey shading indicates highly constrained areas (resolution between 0.7 and 1.0). The values for individual velocities nodes are annotated. The depth uncertainty of the boundaries calculated from the 95 per cent confidence limit of the F-test given in the framed boxes.
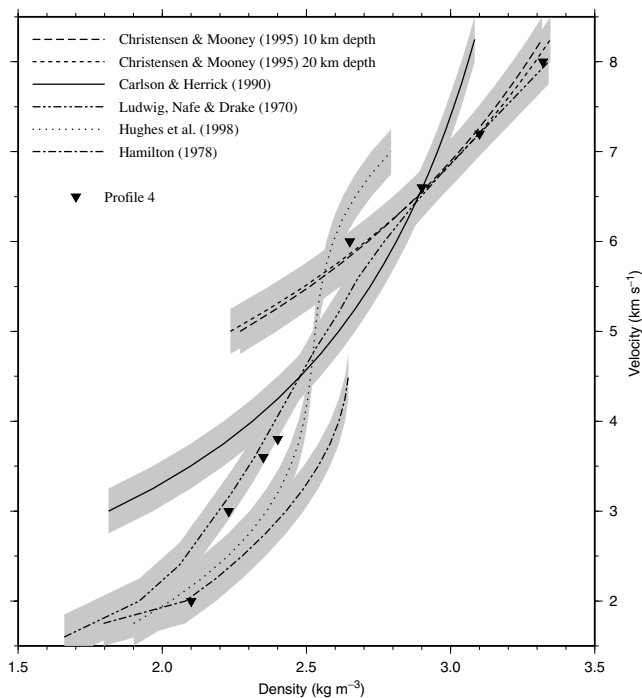

Figure 8. Relationship between velocity and density from Christensen & Mooney (1995) for continental crust, Ludwig *et al.* (1970), Hamilton (1978), Carlson & Herrick (1990) and Hughes *et al.* (1998) for marine sediments. Crosses indicate velocity and corresponding densities used for gravity modelling. Grey shaded areas mark the error bounds of 0.25 g cm^{-3}.

between 6.2–6.4 and 6.6–6.8 km s^{-1} more characteristic for thinned continental or transitional crust between OBS 09 and 12. Only OBS 13 and 14 show velocities and velocity gradients more typical for oceanic crust, as well as a rough basement relief.

This interpretation is also consistent with the free-air gravity anomaly of the area. Profile 4 crosses a strong gravity minimum

with an amplitude of -160 mGal. This minimum is deepest at the foot of the Mazagan plateau and extends 150 km both to the ENE and to the SSW. Oceanic lithosphere in local isostatic equilibrium typically shows a free-air gravity signal fairly close to zero. The lowest gravity minimum corresponds to the portion of the velocity model where the Moho depth increases abruptly from 17 to 24 km, yet the seafloor depth remains nearly constant at approximately 4000 m. This suggests that the gravity minimum may be a geophysical expression of thinned continental crust. The minimum disappears near OBS 11, where the -40 mGal contour is reached and the gravity signature is no longer distinguishable from that of the Seine abyssal plain oceanic domain.

The continental affinity of the crust SE of OBS 7 is clearly expressed by the velocity model, with upper crustal velocities of 5.4–6.2 km s^{-1}. The four high-velocity ridges, with synrift tilted sediments imaged in the coincident MCS profile are typical for tilted basement blocks. This interpretation is confirmed by DSDP drilling data, which penetrated granitic gneiss in the ridge between OBS 5 and 6 (Hinz *et al.* 1984). The velocity effect of these ridges is expressed as undulations in the far-offset arrivals recorded by the land stations (Fig. 4).

Holik *et al.* (1991) find a zone of unusually high seismic velocities in lower crust south of profile 4 (Fig. 9) from sonobuoy refraction seismic data. They interpret these high velocities as underplate, originating from the passage of the Canary hotspot. As the region of high velocity seems to replace the lower crust rather than being located underneath the crust, an alternative explanation of the high velocities might be the existence of serpentinized upper-mantle material in the crust at a magma-starved margin. This zone is broadest south of 33° and disappears around 34.5°, just south of profile 4 perhaps as a result of higher magma production rates during opening. Thus, it cannot be observed in profile 4, but might appear in the profiles perpendicular to profile 4.

Calculation of the spreading rate during early spreading is complicated by the small amplitudes of the magnetic seafloor anomalies produced during the Jurassic magnetic quiet zone. Analyses of a
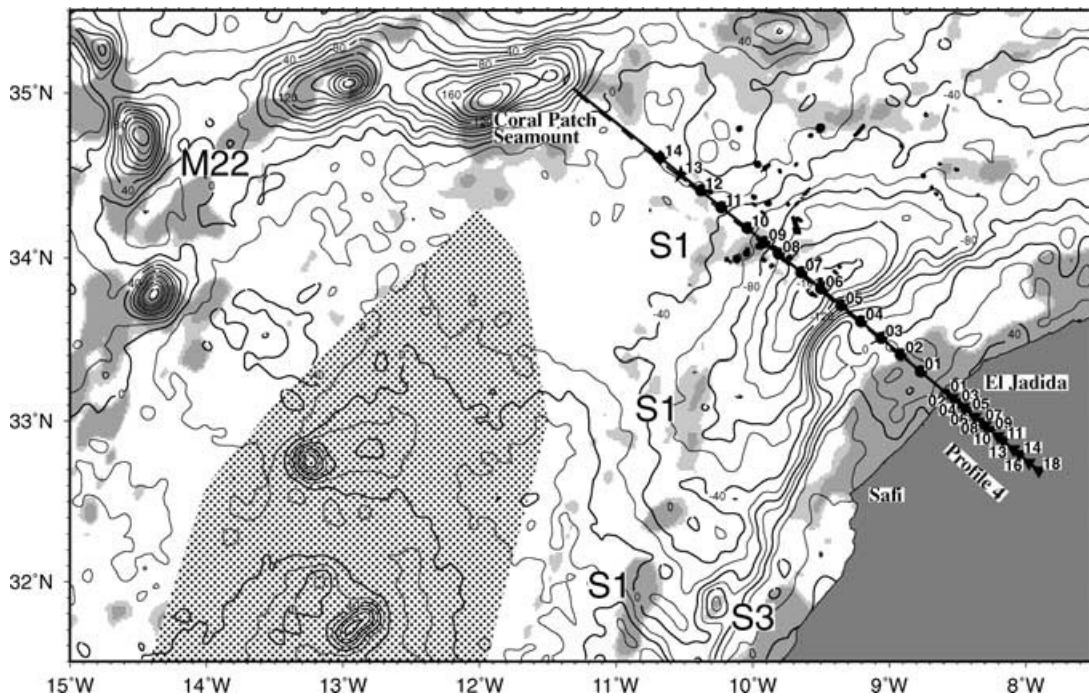
Figure 9. Contoured free-air gravity anomaly of the study area from satellite altimetry with a contour interval of 20 mgal (Sandwell & Smith 1995). Underlain are positive magnetic anomalies between 20 and 100 nT (Verhoef *et al.* 1991). Black polygons mark positions of salt diapirs after Sahabi *et al.* (2004). Stippled area depicts the extent of the zone of unusually high lower crustal velocities from sonobuoy data (Holik *et al.* 1991).
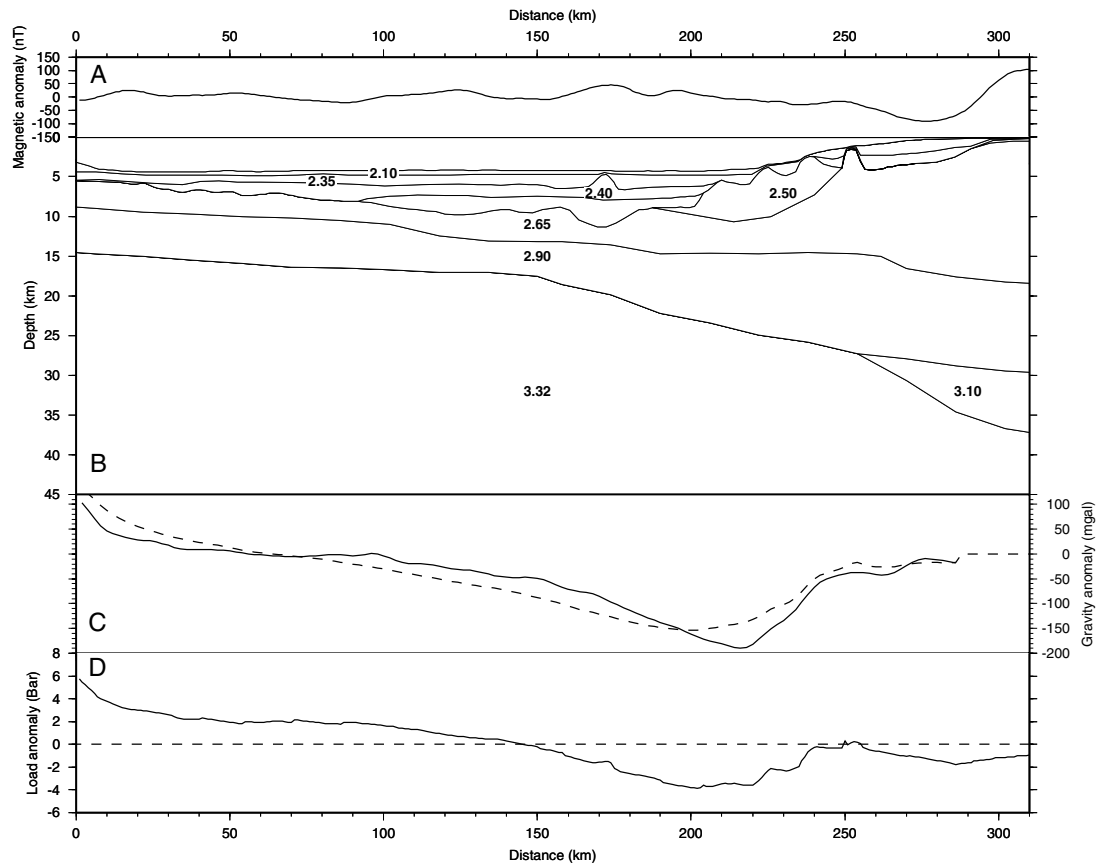

Figure 10. Results of the gravity modelling of profile 4 (Verhoef *et al.* 1991). (a) Magnetic anomaly along the profile. (b) Gravity model boundaries. Densities used during the modelling are annotated. (c) Measured free-air anomaly from satellite altimetry (solid line) (Sandwell & Smith 1995) and predicted anomaly from the modelling (dashed line). A linear trend has been subtracted from the data, because its origin is probably regional, which cannot be reproduced in a smaller scale model. (d) Load anomaly at the Moho. The out-of-plane stresses do not exceed 10 bar, which can be sustained by the crust (Whitmarsh *et al.* 1996).
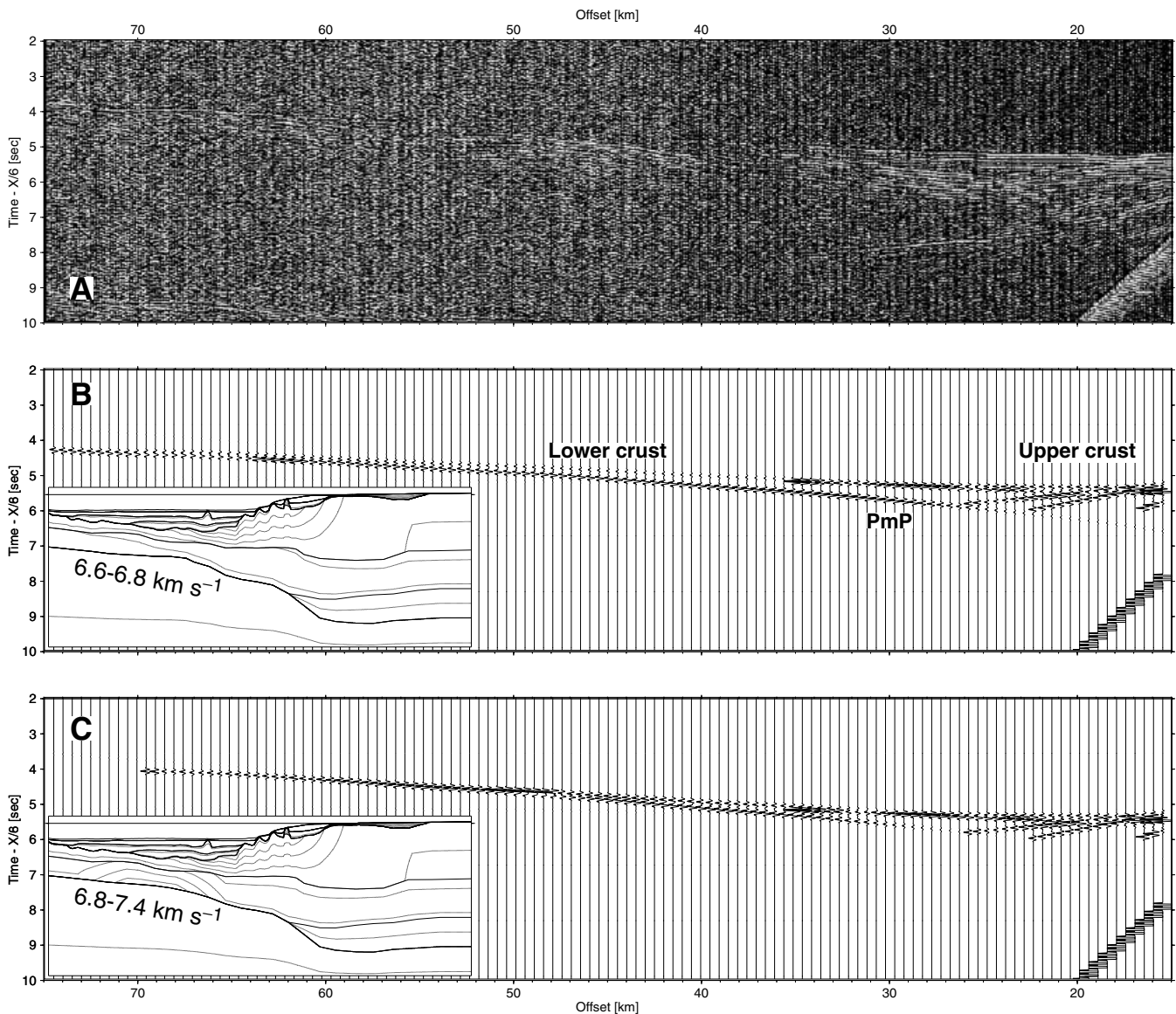
Figure 11. (a) Reduced and bandpass filtered data from OBS 11. (b) Synthetic seismograms calculated using the same parameters as in Fig. 3 and the final velocity model, shown in the inset. (c) Synthetic seismograms calculated using the same parameters as in Fig. 3 and the final alternative velocity model including a zone of anomalous velocities in the lower crust. The model is shown in the inset.

compilation of shipboard magnetic data, including a deep tow gradient magnetometer data in the study area, reveals weak anomalies striking parallel to the high-amplitude anomaly M22 lying to the west (Roeser *et al.* 2002). From the modelling of these anomalies, a half spreading rate of 2.2 cm y^{-1} has been modelled. For comparison, Holik *et al.* (1991) calculated the half spreading rate between anomalies S1 and M25 to be 1.68 cm y^{-1}. Full spreading rates higher than 2 cm yr^{-1} are generally believed to produce normal oceanic crust of a thickness of approximately 7 km (Bown & White 1994). The crust west of the extent of anomaly S1 (OBS 11), believed to mark the onset of ocean floor spreading, shows a thickness of 8 km. This is in good agreement with predictions from numerical studies (Bown & White 1994). However, the crust in this area has been tectonically deformed and has been overprinted by the late Cenozoic igneous activity from Coral Patch and Ampere seamounts (Roeser *et al.* 2002), so the original crustal thickness might well have been lower.

7.2 Comparison to other margins

The lack of synrift magmatism together with the imaged crustal structure (prominent tilted fault blocks, absence of SDRs, etc.) lead us to interpret the Moroccan margin along profile 4 as non-volcanic in nature. A compilation of crustal structure from other non-volcanic margins in the North Atlantic—Iberia domain, indicate a similar overall crustal structure (Dean *et al.* 2000). The width of the extended continental crust for these other margins is typically 100–150 km, while a zone of transitional crust several tens of kilometres wide is commonly observed. This transitional crust is defined as a thin upper crustal layer (less than 3 km thick) with *P*-wave velocity less than 7 km s^{-1} underlain by a high-velocity lower crust (*P*-wave velocity 7.0–7.9 km s^{-1} (Dean *et al.* 2000). While the extended continental domain is 150 km on profile 4, such a transitional crustal domain is not clearly observed in the velocity model. There is a 50-km-wide region of thin crust (6–8 km thick)

from approximately OBS 10 to 13, but lower crustal velocities are slower than those defined as transitional and are thought to represent serpentinized upper mantle. An alternative velocity model (Fig. 11c) with anomalously high lower crustal velocities also provides an adequate fit to the traveltime picks and cannot be ruled out.

There are two possible explanations for the observed absence of transitional crust on the Moroccan margin at 34°N. This zone may be present, but cannot be clearly imaged by our velocity model, as discussed above. Alternatively, a serpentinized upper-mantle domain may form asymmetrically as the result of simple shear in the upper mantle, allowing the lower plate mantle to be exhumed (Wernicke 1985; Chian *et al.* 1995). In this scenario, serpentinized upper mantle would be found on one margin, but would be absent on the other. Published seismic data from the conjugate Nova Scotia margin indicate the presence of anomalous, high-velocity crust (Keen & Potter 1995a). Thus, the Nova Scotia margin may represent the lower plate, where upper-mantle exhumation has occurred.

8 CONCLUSIONS AND OUTLOOK

Wide-angle data from 14 OBS and 14 land stations on the Moroccan margin reveal a transition from 35-km-thick continental crust on the Moroccan platform to 7-km-thick crust over a distance of 150 km. The unthinned continental crust is comprised of three layers of seismic velocities between 5.2–6.4, 6.6–6.8 and 6.8–7.0 km s^{-1}, respectively. Four tilted fault blocks of continental crust comprise the continental slope, where the crust thins from 25 to 15 km. Down to this point, at base of the continental slope, the ratio of upper to lower crustal thickness remains fairly constant (approximately 1 to 1) and thus supports a model of uniform crustal thinning, at least from an initial 35 km thickness to approximately 15 km thickness. At the base of the continental slope sedimentary thicknesses reach 4–6 km, including a 2-km-thick basal layer with a velocity of 4.0–4.5 km. Three uppermost sedimentary layers are locally deformed by salt diapirs. A region of thinned crust approximately 50 km wide marks the transition from continental crust to normal oceanic crust, but this domain does not exhibit the anomalously high *P*-wave velocities typically associated with serpentinized upper mantle and typically found on non-volcanic margins. Normal oceanic crust in the northwestern most 100 km of the model is 7 km thick, consistent with estimated spreading rates of 2 cm yr^{-1} (Holik *et al.* 1991; Roeser *et al.* 2002). The seafloor is gently domed and the sedimentary layers show folding and minor thrust faulting suggestive of basin inversion and compression.

A lateral transition exists in the nature of the Moroccan margin around 33°N. South of this latitude, SDRs have been identified and the S1 magnetic anomaly is strong, both observations having been interpreted as evidence for synrift magmatism. North of this latitude, no SDRs are identified and the prolongation of S1 becomes weak and discontinuous. These observations are mirrored by existing results from the conjugate Nova Scotia margin of North America, where a similar transition from volcanic to non-volcanic margin occurs from south to north, respectively. Detailed work on the deep crustal structure from the Nova Scotia margin is necessary to determine the degree of asymmetry of the rift prior to the initiation of seafloor spreading and to discern which extensional processes formed both margins. Similar studies on the Morrocan margin south of 33°N may shed additional light on the factors controlling the transition from a volcanic to a non-volcanic margin.

REFERENCES

Avedik, F., Renard, V., Allenou, J. & Morvan, B., 1993. 'Single bubble' air-gun array for deep exploration, *Geophysics,* **58,** 366–382.

Bartolome, R., Contrucci, I., Nouze, H., Thiebot, E. & Klingelhoefer, F., 2004. Improving the 'single bubble' multi-channel vertical seismic image with pre-stack depth migration by using the OBS wide-angle reflection/refraction velocities: example of the Moroccan margin, *Geophys. J. Int.,* in press.

Bertrand, H., Dostal, J. & Dupuy, C., 1982. Geochemistry of early Mesozoic tholeites from Morocco, *Earth planet. Sci. Lett.,* **58,** 225–239.

Bown, J.W. & White, R.S., 1994. Variation with spreading rate of oceanic crustal thickness and geochemistry, *Earth planet. Sci. Lett.,* **121**(3–4), 435–449.

Broughton, P. & Trepanier, A., 1993. Hydrocarbon generation in the Essaouira Basin of western Morocco, *Am. Assoc. Petrol. Geol. Bull.,* **77**(6)**,** 999–1015.

Carlson, R.L. & Herrick, C.N., 1990. Densities and porosities in the oceanic crust and their variations with depth and age, *J. geophys. Res.,* **95**(6), 9153–9170.

Chian, D., Louden, K.E. & Reid, I., 1995. Crustal structure of the Labrador Sea conjugate margin and implications for the formation of nonvolcanic continental margins, *J. geophys. Res.,* **100**(12), 24 239–24 253.

Christensen, N.I. & Mooney, W.D., 1995. Seismic velocity structure and composition of the continental crust; a global view, *J. geophys. Res.,* **100**(6), 9761–9788.

Dean, S.M., Minshull, T.A., Whitmarsh, R.B. & Louden, K.E., 2000. Deep structure of the ocean-continent transition in the southern Iberia Abyssal Plain from seismic refraction profiles: The IAM-9 transect at 40° 20′ N, *J. geophys. Res.,* **105**(B3), 5849–4885.

Funck, T., Dickmann, T., Rihm, R., Krastel, S., Lykke-Anderson, H. & Schmincke, H.-U., 1996. Reflection seismic investigations in the volcaniclastic apron of Gran Canaria and implications for its volcanic evolution, *Geophys. J. Int.,* **125**(2), 518–536.

Gutscher, M.-A., Malod, J., Rehault, J.-P., Contrucci, I., Klingelhoefer, F., Victor, L.M. & Spakman, W., 2002. Evidence for active subduction beneath Gibraltar, *Geology,* **30,** 1071–1074.

Hamilton, E.L., 1978. Sound velocity-density relations in the sea-floor sediments and rocks, *J. acoust. Soc. Am.,* **63,** 366–377.

Heyman, M.A.W., 1989. Tectonic and depositional history of the Moroccan continental margin, in *Extensional tectonics and stratigraphy of the North Atlantic margins,* AAPG Mem, Vol. 46, pp. 323–340, eds, Tankard, A.J. & Balkwill, H.R., American Association of Petroleum Geology, Tulsa, OK, USA.

Hinz, K., Dostmann, H. & Fritsch, J., 1982. The continental margin of Morocco: seismic sequences, structural elements and geological development, in *Geology of the Northwest African continental margin,* pp. 34–60, eds K. H. von Rad *et al.,* Springer Verlag, Berlin.

Hinz, K., Winterer, E.L.J. & Party, S.S., 1984. *Initial Reports DSDP 79,* U.S. Government Printing Office, Washington DC.

Hoernle, K. & Schmincke, H.-U., 1993. The role of partial melting in the 15 Ma geochemical evolution of Gran Canaria: a blob model for the Canary hotspot, *J. Petrol.,* **34,** 599–626.

Holbrook, W.S. & Kelemen, P.B., 1993. Large igneous province on the U.S. Atlantic margin and implications for magmatism during continental breakup, *Nature,* **364,** 433–436.

Holbrook, W.S., Reiter, E.C., Purdy, G.M., Sawyer, D., Stoffa, P.L., Austin, J.A., Oh, J. & Makris, J.J., 1994. Deep structure of the U.S. Atlantic continental margin, offshore South Carolina, from coincident ocean bottom and multichannel seismic data, *J. geophys. Res.,* **99,** 9155–9178.

Holik, J.S., Rabinowitz, P.D. & Austin, J.A., 1991. Effects of the Canary hotspot volcanism on the structure of oceanic crust off Morocco, *J. geophys. Res.,* **96,** 12 039–12 067.

Hughes, S., Barton, P.J. & Harrison, D., 1998. Exploration in the Shetland-Faeroe Basin using densely spaced arrays of ocean-bottom seismometer, *Geophysics,* **63**(2), 328–334.

Keen, C.E. & Potter, D.P.K., 1995. Formation and evolution of the Nova Scotia rifted margin: Evidence from deep seismic reflection data., *Tectonics,* **14**(4), 918–932.

Keen, C.E. & Potter, D.P.K., 1995. The transition from a volcanic to a nonvolcanic rifted margin off eastern Canada, *Tectonics,* **14**(4), 359–371.

Klitgord, K.D. & Schouten, H., 1986. Plate kinematics of the central Atlantic, in *The Geology of North America, the western North Atlantic region.* pp. 351–378, eds Vogt, P.R. & Tucholke, B.E. GSA, Boulder, CO, USA.

Le Roy, P., Guillocheau, F., Pique, A. & Morabet, A.M.C., 1998. Subsidence of the Atlantic Moroccan margin during the Mesozoic, *Can. J. Earth Sci.,* **35,** 476–493.

Ludwig, J.W., Nafe, J.E. & Drake, C.L., 1970. Seismic refraction, *The Sea,* **4**(1), 53–84.

McKenzie, D., 1978. Some remarks on the development of sedimentary basins, *Earth planet. Sci. Lett.,* **40,** 25–65.

Miller, D.J. & Christensen, N.I., 1997. Seismic velocities of lower crustal and upper mantle rocks from the slow-spreading Mid-Atlantic Ridge, south of Kane Transform MARK. In: *Proc. Ocean drill. Program Sci. results,* Vol. 153, pp. 437–454. Texas A&M University, College Station, TX, USA.

Mutter, J.C., 1993. Margins declassified, *Nature,* **364,** 393–394.

Pedley, R.C., Busby, J.P. & Dabek, Z.K., 1993. GRAVMAG *user manual - interactive 2.5d gravity and magnetic modelling.* Technical Report WK/93/26/R, British Geological Survey, Keyworth, Nottingham.

Roeser, H.A., 1982. Magnetic Anomalies in the Magnetic Quiet Zone off Morocco, in *Geology of the Northwest African Continental margin,* Vol. 107, pp. 61–68, eds von Rad, U. *et al.,* Springer Verlag, Berlin.

Roeser, H.A., Steiner, C., Schreckenberger, H. & Block, M., 2002. Structural development of the Jurassic Magnetic Quiet Zone off Morocco and identification of Middle Jurassic magnetic lineations, *J. geophys. Res.,* **107,** X-1–X-23.

Ruellan, E. & Auzende, J.-M., 1985. Structure et evolution du plateau sous-marin de El Jadida (Mazagan, Ouest Maroc), *Bull. Soc. Geol. France,* **1,** 103–114.

Sahabi, M., Aslanian, D. & Olivet, J.-L., 2004. Un nouveau point de départ pour l'histoire de l'Atlantique central, *Compte Rendus Geoscience,* **336,** 12, 1041–1052.

Sandwell, D. & Smith, W., 1995. *Marine gravity from satellite altimetry,* The Geological Data Center, Scripps Institution of Oceanography, La Jolla, CA (digital file, version 7.2), anonymous ftp to www.baltica.ucsd.edu

Sartori, R., Torelli, L., Zitellini, N., Peis, D. & Lodolo, F., 1994. Eastern segment of the Azores-Gibraltar line 'Central Eastern Atlantic': A an oceanic platte boundary with diffuse compressional deformation, *Geology,* **22,** 555–558.

Smith, W. & Sandwell, D., 1997. Global seafloor topography from satellite altimetry and ship depth soundings, *Science,* **277,** 1956–1962.

Verhoef, J., Collette, B.J., Dañobeitia, J.J., Roeser, H.A. & Roest, W.R., 1991. Magnetic anomalies off West-Africa, *Mar. geophys. Res.,* **13,** 81–103.

Weigel, W., Wissman, G. & Goldflam, P., 1982. Deep seismic structure (Mauritania and central Morocco), in *Geology of the northwest african continental margin,* Vol. 8, pp. 132–159, eds Von Rad, U., Hinz, K., Sarntheim, M. & Seibold, E. Springer Verlag, Berlin, Heidelberg, New York.

Welsink, H.J., Dwyer, J.D. & Knight, R.J., 1989. Tectono-stratigraphy of the passive margin off Nova-Scotia., in *Extensional tectonics and stratigraphy of the North Atlantic margins,* AAPG Mem, Vol. 46, pp. 215–231, eds Tankard, A.J. & Balkwill, H.R., American Association of Petroleum Geology, Tulsa, OK, USA.

Wernicke, B., 1985. Uniform-sense normal simple shear of the continental lithosphere, *Can. J. Earth Sci.,* **22,** 108–125.

Wessel, P. & Smith, W.H.F., 1995. A new version of the Generic Mapping Tool (GMT), *EOS, Trans. Am. geophys. Un.,* **76,** 329.

White, R.S. *et al.,* 1987. Hatton Bank (northwest U.K.) continental margin structure, *Geophys. J. R. astr. Soc.,* **89,** 265–272.

Whitmarsh, R.B., White, R.S., Horsefield, S.J., Sibuet, J.-C., Recq, M. & Louvel, V., 1996. The ocean-continent boundary off the western continental margin of Iberia: crustal structure of Galicia Bank, *J. geophys. Res.,* **101,** 28 291–28 314.

Ye, S., Canales, J.-P., Rihm, R., Danobeitia, J.-J. & Gallart, J., 1999. A crustal transect through the northern and northeastern part of the volcanic edifice of Gran Canaria, Canary Islands, *J. Geodynamics,* **28**(1), 3–26.

Zelt, C.A. & Ellis, R.M., 1988. Practical and efficient ray tracing in two-dimensional media for rapid travel time and amplitude forward modelling, *Can. J. Explor. Geophys.,* **24,** 16–34.

Zelt, C.A. & Smith, R.B., 1992. Seismic travel time inversion for 2-D crustal velocity structure, *Geophys. J. Int.,* **108,** 16–31.